

DIAGNOSTIC TECHNIQUES FOR HIGH TEMPERATURE PLASMA REACTIONS*

J. H. Mullen, J. M. Madson, L. N. Medgyesi-Mitschang, T. C. Peng, P. M. Doane

McDonnell Douglas Research Laboratories
McDonnell Douglas Corporation
St. Louis, Missouri 63166

Introduction

Numerous experimental techniques have been employed in the study of interactions between charged and neutral constituents of a plasma. The particular technique employed in any experiment has been determined by the phenomena under investigation. In particular, beam and drift tube experiments as well as afterglow techniques have been used to study phenomena such as ionization, electron recombination and electron attachment in a temperature range near room temperature. Some recent measurements on the electron attachment process have been made at elevated gas temperatures where the reaction products were analyzed with a mass spectrometer^{1,2,3}. The usual limitation on the gas temperature in these experiments is the maximum working temperature of the material used for the target gas heater. Electron recombination, electron attachment and ion-molecule reaction processes in plasmas have also been studied using a flowing afterglow technique^{4,5}. This technique has an advantage over the stationary afterglow method for reaction rate studies in that it permits the injection of target molecules into a flowing plasma stream without subjecting these molecules to the main discharge excitation mechanisms. However, temperatures used in flowing afterglow studies have usually been less than 600°K. To study these processes at higher temperatures and in particular temperatures encountered by reentry vehicles (2000 - 4000°K), plasma discharges having these high temperatures must be employed. For these studies arc heated plasma sources have been used with both subsonic channel flows⁶ and supersonic free jets^{7,8}. Interpretation of experimental results is difficult with both of these techniques because of the inhomogeneity of plasma parameters in the reaction region. The system described in this paper encompasses the desirable aspects of the above mentioned approaches and enables quantitative reaction rate measurements to be made⁹.

Overall System Description

The experimental apparatus shown in Fig. 1 is composed of a plasma source, chemical reaction channel, expansion region and mass analysis chamber. The gases, heated in an electrodeless induction plasma discharge, react with supersonically injected target molecules in a sonic reaction channel and are subsequently "chemically frozen" by rapid expansion in a free molecular jet. The electron density, excitation temperature, electron temperature, and gas temperature of the plasma at the source is measured with an optical spectrometer, an X-band microwave radiometer, and high temperature thermocouples. In addition, excitation temperatures are also measured in the reaction channel. Free electron number densities and ion-molecule intensities in the free expansion region are measured simultaneously with a Ka-band microwave interferometer and a free jet ion-molecular beam mass sampling system using a quadrupole mass spectrometer. The design, construction and particulars of the plasma system and instrumentation will be described subsequently.

*This research was conducted under McDonnell Douglas Independent Research and Development Program

Figure 1 Schematic Drawing of Experimental Apparatus

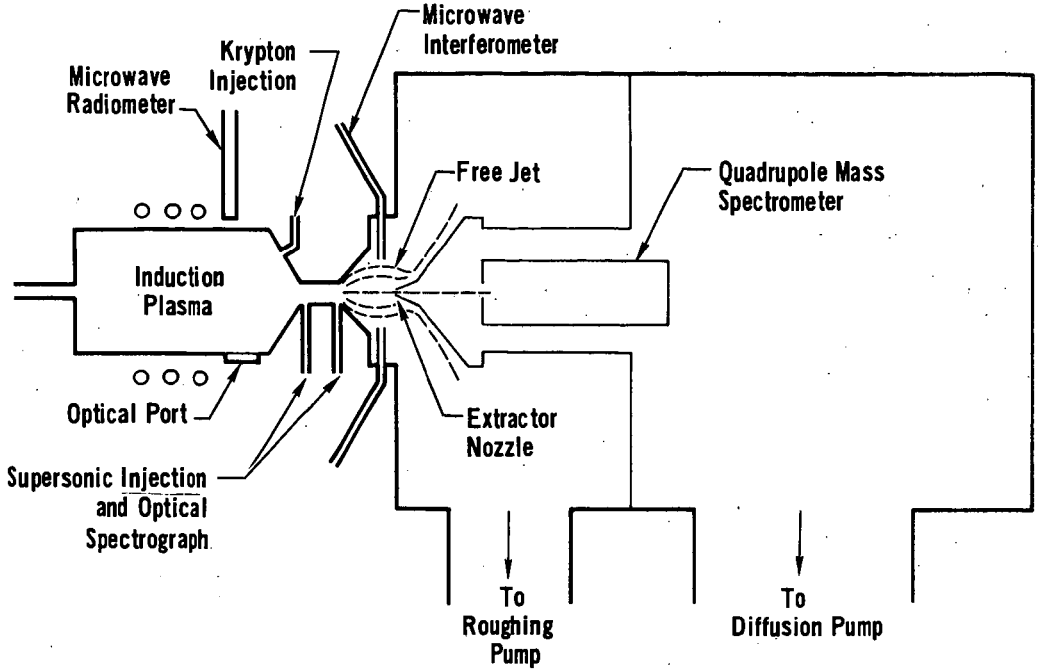
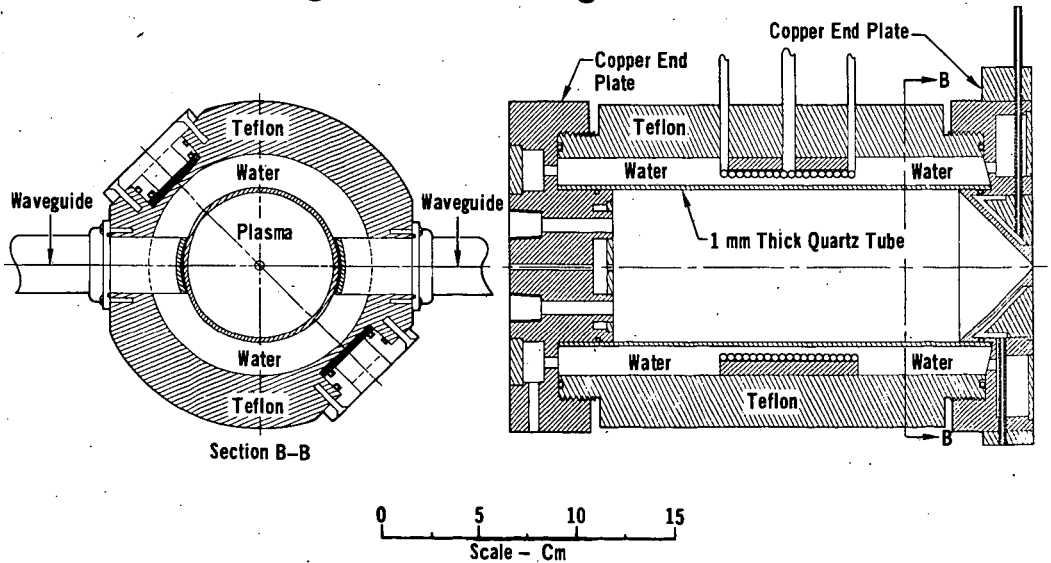


Figure 2 rf Discharge Chamber



Plasma Source

An electrodeless induction plasma similar to those of Reed¹⁰ and Eckert, et al¹¹ is used as the plasma source. A 0 to 100 kW, class C, rf oscillator operating at 1 MHz is used to supply the plasma heating power. This plasma source eliminates electrode contamination of the plasma in the chemical reaction channel and permits uniform heating of the plasma with electron temperatures close to the gas temperature in the central core region. A scale drawing of the discharge tube is shown in Fig. 2. The 80 mm diameter plasma discharge tube is made of 1 mm thick quartz, approximately 160 mm long. The ends are made to fit the O-ringed copper end pieces by padding standard diameter quartz tubes on machined carbon mandrils mounted in a glass blowing lathe. Allowance has to be made for the expansion of the carbon during this step. The end plates (threaded for assembly to the water jacket) are made of copper and are water cooled. The water jacket is machined from a 203 mm O.D. - 101 mm I.D. cast Teflon tube and handles a 1.14 l/sec flow rate. Two oppositely wound, eight turn coils of 3 mm O.D. copper tubing surround the plasma discharge tube and are mounted collinerly inside the water jacket. A 1.5 mm clearance between the discharge tube and the water jacket gives adequate coolant water flow. To prevent rf sputtering between the coils and the copper end plates, the coils are center fed and grounded at the ends so that the rf plasma potential is minimum at each end of the discharge. In this configuration, the quartz plasma tubes have operated for more than 100 hours before failure.

In operation, the plasma is initiated at low power at 10^{-3} to 10^{-1} Torr pressure. After initiation the discharge can be operated from 1 to 760 Torr at oscillator power inputs ranging from 1 to 69 kW using argon. On air the discharge can be operated from 1 to 600 Torr with power inputs from 20 to 100 kW. At low oscillator power inputs (i.e. < 39 kW) a tungsten rhenium thermocouple is used to measure the local gas temperature of the plasma at the entrance to the plasma channel. These measured temperatures for various argon mass flow rates are shown in Fig. 3 as a function of source pressure. The source pressure is controlled by changing the oscillator power input. Above 2850°K the thermocouple melted. The dashed lines represent theoretically predicted curves based on gas dynamic considerations. The deviation at the higher mass flow rates and high temperatures apparently is due to bending of the thermocouple from the center of the channel. Gas temperature data above this range is difficult to obtain. However, by monitoring the source pressure at higher powers the temperature can be predicted from the theoretical curve. Because the gas is sonic at the thermocouple, the temperature derived from Fig. 3 must be multiplied by 1.33 to obtain the source chamber temperature. The highest operating chamber pressures are indicated by a star in Fig. 3 and show the maximum temperatures obtainable. These points were limited by the maximum plate current of the oscillator triode (10 amperes) rather than the maximum power capability of the triode itself. An improvement in power output is possible by reducing the number of turns on the plasma coil. When gas mixtures such as air which contain diatomic molecules are used, loading of the oscillator is sufficiently low so the maximum plate current coincides with maximum power. The design described here is a compromise that provides operation on monatomic as well as diatomic gases without mechanical or electrical modifications. Table I shows typical operating conditions for the plasma source operating on argon and air.

Optical Spectrographic Measurements

To interpret the chemical reactions in the channel it is necessary to know the electron temperature of the plasma in the source and reaction channel. In most electric discharges there is some degree of nonequilibrium between the electron and gas temperatures. Simple techniques such as thermocouples can not be used to determine both of these temperatures because the energy in the free electrons represents only a small fraction of the total energy in the gas. Langmuir probes were not

Figure 3 Channel Gas Temperatures

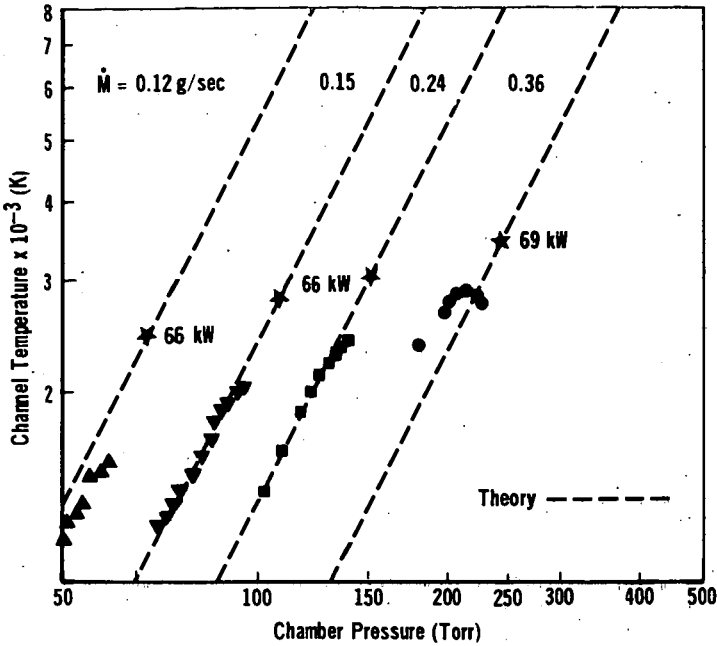


Figure 4 Radiometer Schematic

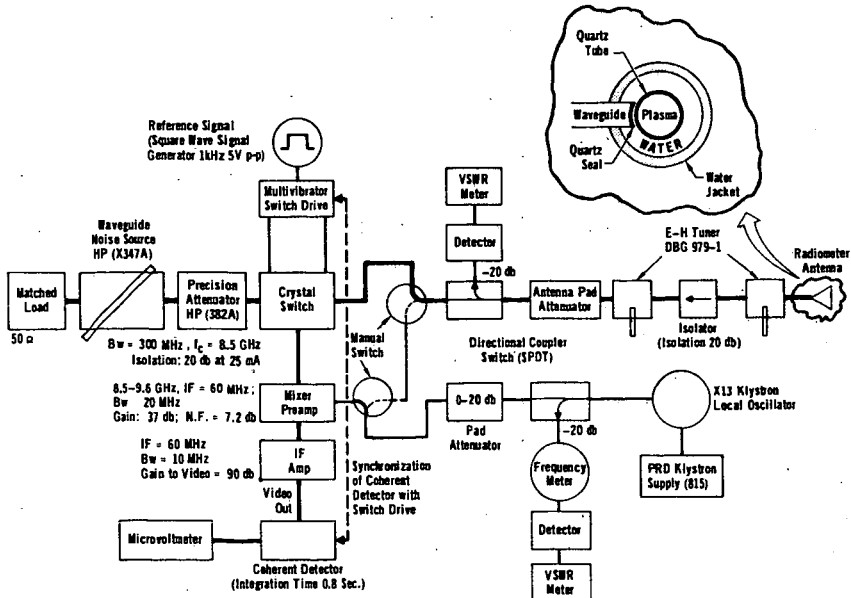
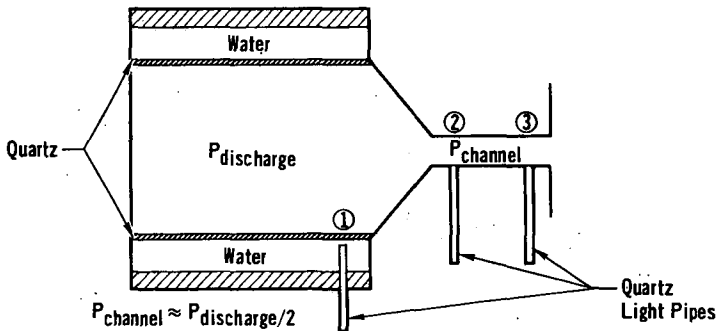


Table I Typical rf Plasma Operating Conditions

| Line Power (kW) | M g/sec | Discharge Pressure (Torr) | Plate | | Grid | | Filament | | rf Generator Efficiency (%) | Gas |
|-----------------|---------|---------------------------|--------|---------|--------|---------|----------|---------|-----------------------------|-------|
| | | | V (kW) | I (Amp) | V (kV) | I (Amp) | V (Volt) | I (Amp) | | |
| 90 | 0.104 | 165 | 8.5 | 10 | 1.0 | 0.94 | 12.7 | 195 | 58.0 | Air |
| 85 | 0.130 | 206 | 8.5 | 9.5 | 1.13 | 1.00 | 12.7 | 195 | 58.5 | Air |
| 95 | 0.163 | 258 | 9.2 | 9.7 | 1.25 | 1.14 | 12.8 | 200 | 60.9 | Air |
| 100 | 0.326 | 542 | 10 | 9.8 | 1.55 | 1.40 | 12.8 | 200 | 62.0 | Air |
| 6 | 0.193 | 139* | 2.8 | 2.55 | 0.07 | 0.06 | 12.8 | 200 | ~50 | Argon |
| 24 | 0.193 | 166* | 4.5 | 5.1 | 0.27 | 0.18 | 12.8 | 200 | ~50 | Argon |
| 66 | 0.193 | 164 | 6.55 | 9.65 | 0.74 | 0.30 | 12.8 | 200 | ~50 | Argon |
| 69 | 0.273 | 247 | 6.65 | 9.85 | 0.77 | 0.31 | 12.8 | 200 | ~50 | Argon |

*With Thermocouple in Channel

Table II Spectrographically Measured Excitation Temperatures



| Discharge Chamber Pressure (Torr) | T ₁ Chamber Temperature (K) | T ₂ Channel Upstream Temperature (K) | T ₃ Channel Downstream Temperature (K) |
|-----------------------------------|----------------------------------------|-------------------------------------------------|---------------------------------------------------|
| 51.7 | 8820 | 5560 | 5600 |
| 103 | 8540 | - | - |
| 155 | 8480 | 5260 | 5390 |
| 310 | 11810 | 6020 | - |
| 465 | 10326 | - | 5350 |
| 620 | 8510 | 6410 | 4120 |

used because of the difficulty involved in inserting them into the source and interpreting the resulting data. Furthermore, any perturbation introduced by them in the discharge region causes devitrification and rapid failure of the quartz tube. Optical spectrographic techniques^{12,13,14} were found to be applicable.

Spectrographic observations of the plasma at the source and at two axial positions in the reaction channel were made. Aluminized quartz light pipes were used to direct the light to a one-meter (Jarrell Ash Model 78-466) spectrograph. Excitation temperatures were obtained at the three positions and for various flow conditions shown in Table II. The discharge chamber temperature at 310 and 465 Torr are thought to be in error as a result of a discharge instability in this pressure range and the slow response of the strip chart recorder. The excitation temperatures were obtained from Boltzmann plots of Ar I line intensities. The entire optical system (including the light pipes) was calibrated between 5000 and 4000 Å using a tungsten ribbon filament lamp.

In the optical measurements, the excitation temperature was assumed to be close to the electron temperature due to the efficient energy exchange between free electrons and the upper bound electronic states. Electron density measurements were attempted using line profile and continuum techniques. Plasma source operating conditions were 114 Torr and 51 kW of rf power. No line broadening was detected indicating that the electron densities were less than 1.0×10^{16} e/cm³. The electron density calculated from the Kramers - Unsöld equation for continuum radiation was 1.5×10^{16} e/cm³.

Microwave Radiometer Measurements

In addition to the optical spectrographic excitation temperature measurements of the plasma source the electron temperature was measured using radiometric techniques. As is known the emitted spectrum of any homogeneous source becomes more continuous as the depth of the source increases, since initially the strongest lines tend to be reabsorbed, then the weaker ones, and eventually all parts of the continuum until the spectrum resembles a blackbody continuum¹⁵. However, in the laboratory this happens at best over a rather limited frequency range. (If this were not the case, radiative energy losses would be formidable.) Ordinarily in the microwave frequency range no line spectra are present and only continuum radiation occurs. In laboratory plasmas with plasma frequencies above the radiometer frequency considerable reflection of the continuum radiation at the plasma-air interface occurs resulting in very low levels of radiated power.

For the radiometric measurements a modified Dicke X-band microwave radiometer operated at 8.5 GHz shown in block diagram form in Fig. 4 was used^{16,17,18}. In operation the radiometer is electronically switched between the plasma source and a standard noise source. A standard noise source and a 50 dB precision attenuator combination form a 10,000°K calibrated blackbody temperature standard against which the temperature of the plasma is compared. The difference in thermal radiation between the plasma and the standard is detected, amplified, and processed by the radiometer as follows^{19,20}. The signal is passed through a balanced low-noise mixer IF pre-amp combination, followed by a high gain IF amplifier. This is followed by a coherent detector in synchronism with the electronic X-band switch and the output is read on a precision microvoltmeter²¹.

The radiometer receiving antenna is a contoured open-ended waveguide, capped by a similarly contoured 1.5 mm thick quartz window (Fig. 2). The waveguide is oriented so that the E-plane is parallel to the axis of the discharge chamber, resulting in the smallest amount of mismatch. Because of the small radiation signal from the source, this mismatch was tuned out.

To accomplish this, the following modifications were adopted from the conventional radiometer. Provision was made to operate the system in a non-radiometer mode via a "test loop". In this mode, the local oscillator (L.O.) signal is passed directly to the radiometer antenna through a set of manual switches by-passing the remainder of the circuit, allowing simple transmission and reflection measurements to be made. Due to the high plasma density ($N_e > 10^{15}$ e/cm³), no transmitted signal through the plasma could be measured as signal attenuation exceeded 60 dB. The E/H tuner closest to the antenna was adjusted for maximum noise signal in the usual radiometer mode with the discharge operating at 150 Torr. The other E/H tuner was tuned for minimum reflected signal in the test loop mode to eliminate any reflections at the isolator.

The fine adjustment of the radiometer was accomplished in the usual radiometer mode with the antenna attenuator set at maximum and the phase and amplitude of the reference signal in the coherent detector adjusted for maximum deflection on the microvoltmeter.

With the radiometer system adjusted for maximum sensitivity and the antenna network tuned and matched, the radiometer was used for electron temperature determination. The radiation power incident upon the radiometer may be expressed analytically as

$$P = kBT = kB(1-\Gamma) T_p = kB(1-\Gamma) AT_r$$

so that

$$T_r = \frac{P}{kB(1-\Gamma) A}$$

where $k = 1.38 \times 10^{-23}$ joules/°K (Boltzmann's constant); B is the bandwidth of the incident radiation (Hz); Γ is the reflection coefficient due to the mismatch introduced by the antenna window, the quartz plasma jacket, and the water gap; T , T_p and T_r are the effective blackbody temperature, plasma blackbody temperature and radiation temperature respectively; A is the absorption coefficient (i.e. equal to the emissivity) which includes reflections at the plasma quartz interface and the plasma absorption.

By proper matching of the radiometer antenna, $\Gamma = 0$. The radiation temperature is obtained by setting the precision attenuator in the reference leg so that the radiometer output (on the microvoltmeter) is nulled. In this way a balance is achieved between the plasma and reference leg signals and consequently between the equivalent noise temperatures of the plasma and the standard noise source. The decibel reading on the precision attenuator yields T_p via the calibration curve which relates the equivalent blackbody temperature to the attenuator setting. From this temperature the electron radiation temperature T_r can be obtained if A is known. The radiation temperature equals the electron temperature T_e when the electrons are Maxwellian distributed. Past measurements have shown that the plasma is in equilibrium, at least in the LTE sense, so that the assumption of a Maxwellian distribution is reasonable for the electrons and thus T_r is assumed equal to T_e .

To relate T_p to T_r (and hence T_e), the emissivities were calculated for a slab plasma for a given discharge pressure (P_t), fraction of ionization (p) and T_e . In these calculations the electron-ion and electron-neutral interactions were included, using Appleton-Bray²² for the former and Brown's cross section data²³ for the latter. For the range of N_e between 10^{10} and 5×10^{16} e/cm³ and T_e less than 18,000°K, the electron-ion collisions were found to be dominant. Representative results from these computations for the emissivity as a function of the fraction of ionization

are given in Fig. 5. If the electron density measured with the microwave interferometer is used ($5 \times 10^{15} \text{ e/cm}^3$) to calculate ϵ the resulting electron temperature agrees with the spectrographically measured temperature (Fig. 6).

Reaction Channel Design

The reaction channel for this system was designed so the plasma chemistry could be most easily interpreted. The channel was made sufficiently long for reaction rates to be determined but not long enough for an appreciable boundary layer buildup or for fully development pipe flow. A well established result of fluid mechanics is that for Reynolds numbers below 2300, flow through a channel will remain laminar even in the presence of strong disturbances in the flow prior to its entrance²⁴. The Reynolds number for the channel is

$$R_e = \frac{\rho \bar{u} D}{\mu}$$

where ρ = density of flow in channel,
 \bar{u} = average velocity,
 D = channel diameter,
 μ = viscosity of flow in channel.

Using the mass flow relationship $\dot{m} = \rho u A$, where A = channel cross section,

$$R_e = \frac{4\dot{m}}{\pi D}$$

Typical operation conditions are

$$\begin{aligned} \dot{m} &= 0.23 \text{ g/sec} \\ D &= 0.4 \text{ cm} \\ \mu &\approx 1.1 \times 10^{-3} \text{ (assuming a } T^{1/2} \text{ temperature dependence and } 3000^\circ\text{K)}. \end{aligned}$$

The resulting Reynolds number is approximately 700 indicating laminar flow. Experimentally the flow can be made turbulent by increasing the mass flow rate to approximately 1.00 g/sec.

The velocity profile in the transient or inlet portion of a circular channel for laminar flow has been investigated experimentally by Nikuradse²⁵. Only after approximately 50 channel diameters downstream would the flow velocity be described by Hagen-Poiseuille pipe flow. Using the results of Nikuradse, velocity profiles at several stations for a 1.6 cm channel are shown in Fig. 7. The velocity profile is shown to be nearly flat at the end of the channel indicating no appreciable boundary layer buildup.

Target Gas Injection and Mixing

The target gas injection system is composed of a high pressure reservoir, regulator, pressure gauge, needle valve and supersonic orifice mounted in the wall of the channel near the entrance. The orifices are commercially available pinholes, made of 25 μm thick nickel ranging from 35 to 200 μm in diameter. These orifices are silver soldered to stainless steel tubes and mounted in the channel. The orifice is operated above the critical pressure ratios P_u/P_c (upstream pressure/channel pressure) so target gas injection is always supersonic. If the channel gas were not flowing the position of the first Mach disc would be

$$X = 0.67 D \sqrt{P_u/P_c}$$

Figure 5 Microwave Emissivity at 8.5 GHz

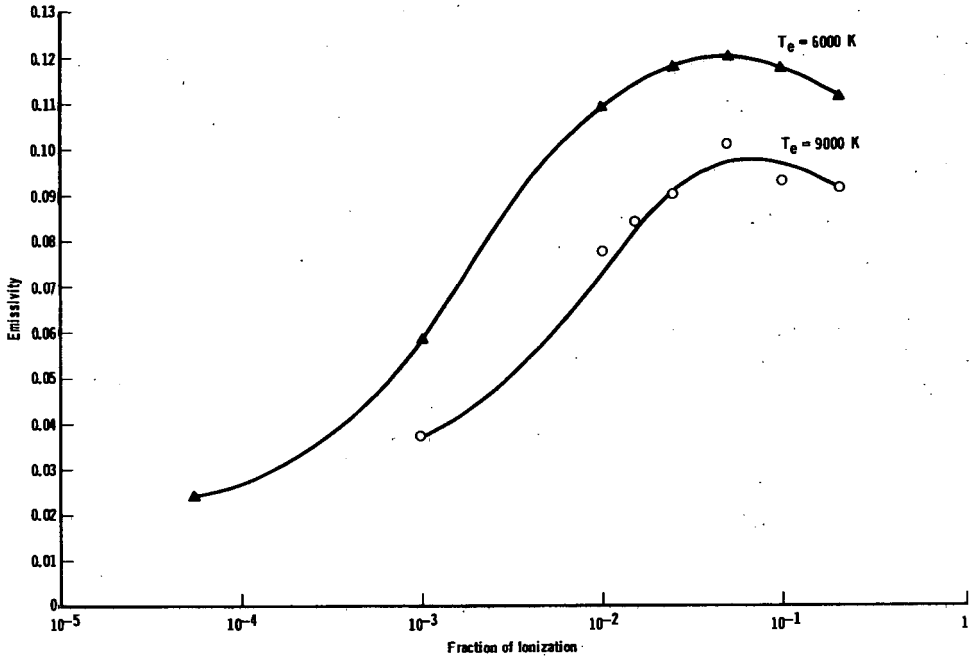


Figure 6 Source Electron Temperature

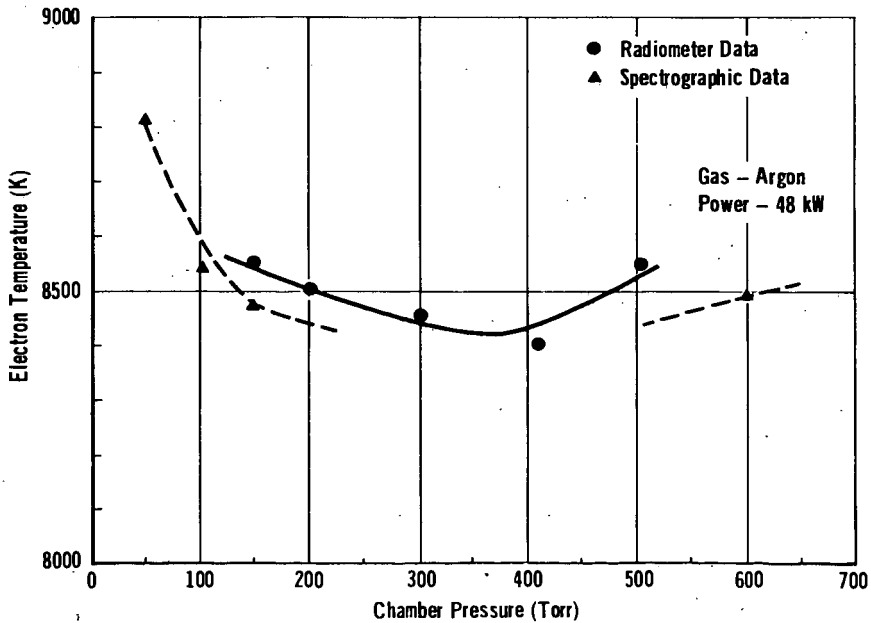


Figure 7 Channel Velocity Profile

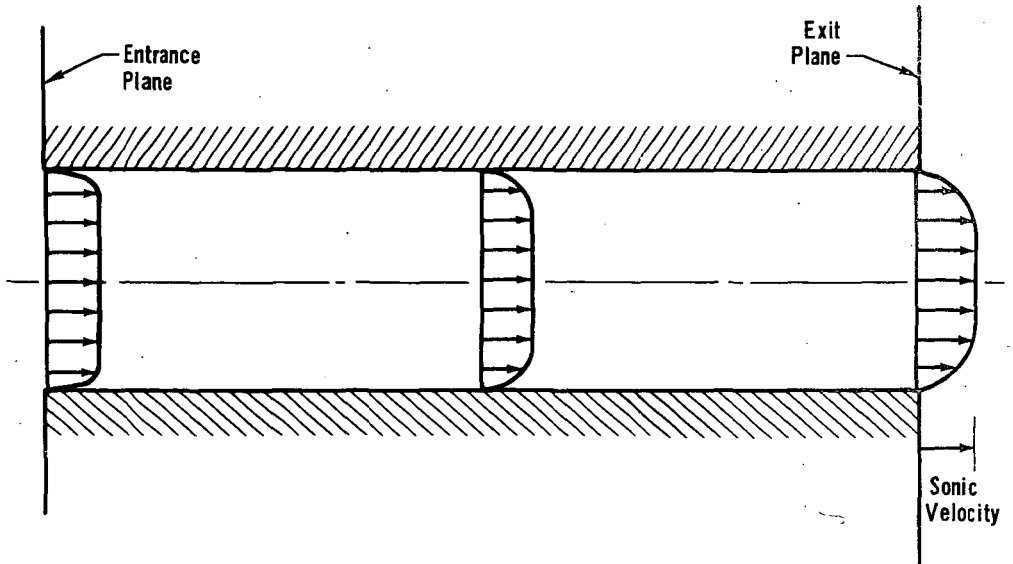
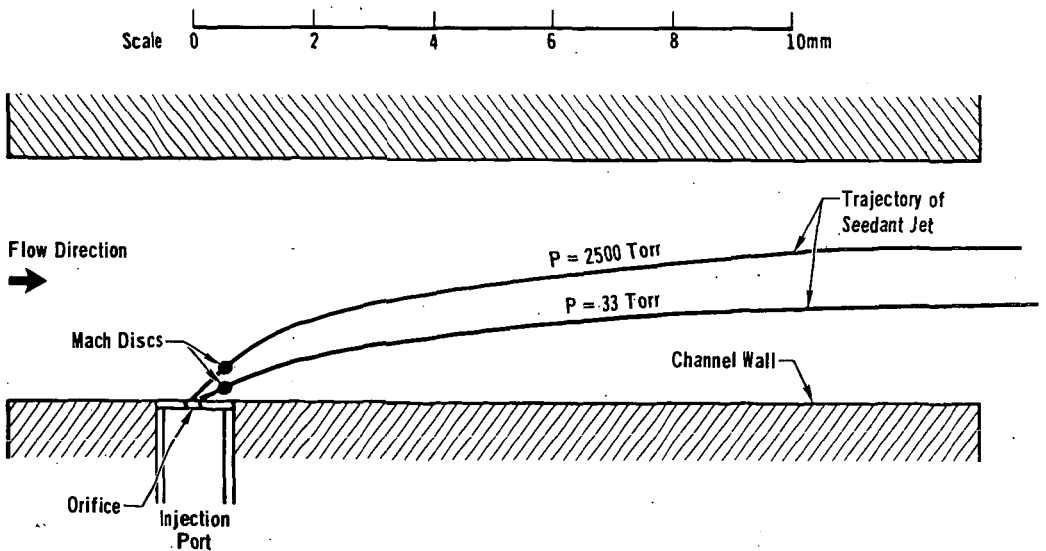


Figure 8 Target Gas Injection



where X = Mach disc distance from orifice, and
 D = orifice diameter.

However, the plasma in the reaction channel is traveling at sonic velocity which makes the mixing problem much more difficult. Shandorov²⁶ and Ivanov²⁷ have developed an empirical expression for the trajectory of the deflected jet based on experimental studies. They have investigated a range of dynamic pressure ratios from 2 to 22 and for 45° to 90° range of angles between initial injection flow and channel flow. The centerline for two dynamic pressure ratios calculated from these expressions is shown in Fig. 8 as dashed lines. Using the Mach disc location along this centerline and Mach disc diameter given by Crist, et al²⁸,

$$\frac{D_m}{D_j} = 0.22 (P_u/P_c)^{2/3},$$

where D_m = diameter of Mach disc, and
 D_j = diameter of orifice,

the Mach disc is shown superimposed for a 200 μ m orifice. The nature of the flow after the Mach disc is probably free turbulent flow. The lifetime of this turbulent flow is uncertain, since the channel main flow is strongly laminar ($Re \approx 700$) and will eventually damp out the turbulence.

From this target gas injection analysis, it is apparent that care must be taken in interpreting chemical reactions in the channel. Rate constants evaluated from this experiment also include mixing rates. However, since the \ln of the electron density as a function of target molecule density is linear over a large range mixing appears to be no problem. The mixing could obviously be improved by using three injection nozzles around the circumference of the channel spaced every 120°. This modification is presently being incorporated.

Expansion Flow Field

The plasma and reactants pass from the reaction channel into an expansion chamber evacuated by 141.5 l/sec vacuum pump. For an argon mass flow of 0.22 g/sec, and a discharge pressure of 165 Torr, the pressure in the expansion chamber is 0.26 Torr. The channel pressure is maintained at approximately 87 Torr. These were the conditions at which most of the present plasma chemistry experiments were performed. The expansion flow is a free jet for which the flow field has been substantially investigated²⁹. For the above operating conditions the free jet expansion has a theoretical Mach disc location of 12.2 nozzle diameters (4.85 cm) downstream from the channel exit. However, this theoretical location is based on experimental verifications for a single component gas expansion. Thus for a plasma, the theoretical location of Mach disc is only indicative of a general distance near which the real Mach disc is likely to be present. In our experiment, a visual observation indicates a probable location for the Mach disc at 5.71 cm downstream from the channel exit. This is also the location for the extractor nozzle through which the plasma sampling is made.

As in the case of the Mach disc calculation, the thermodynamic, fluiddynamic and collision parameters in the free jet flow field have been calculated from the known correlations of single component gas free jet experiments (Fig. 9) due to the lack of established experimental correlations for a plasma free jet.

The calculated terminal Mach number is 14.26 and is located at $X/D = 9.25$ on the free jet axis (Fig. 10a), indicating that there will be no interference from interparticle collisions at the extractor nozzle location at $X/D = 14.4$. In the

Figure 9 Expansion Flow Field

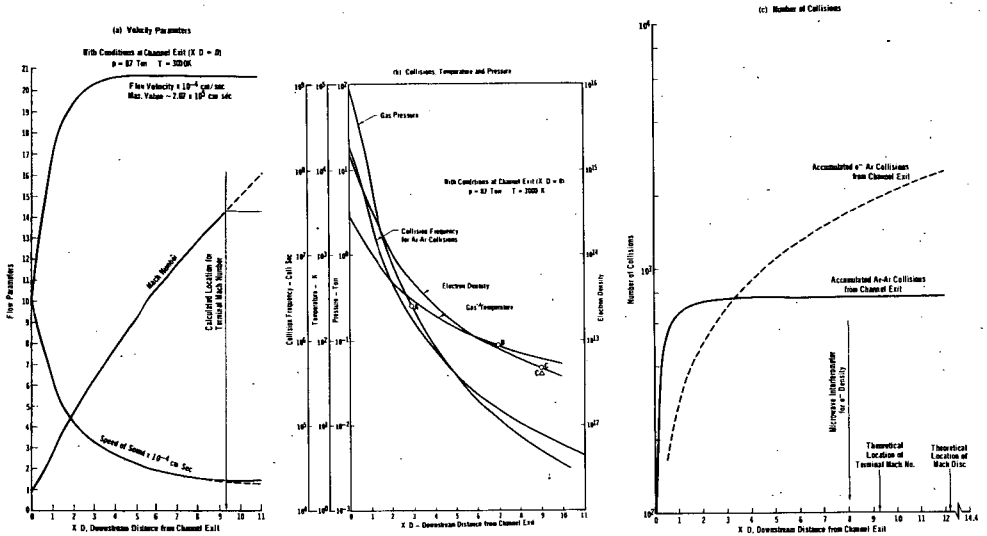
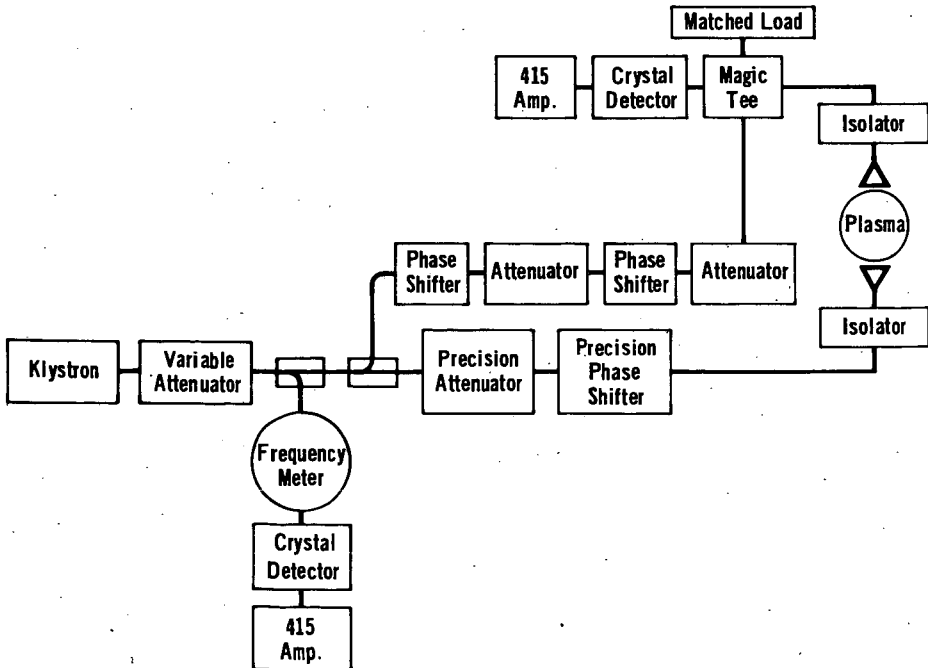


Figure 10 Ka-Band Microwave Interferometer



free jet before the terminal Mach number, the flow field is a collision dominated laminar flow closely described by isentropic relations. Calculations indicate that the environmental pressure level (0.26 Torr) is reached at $X/D \approx 3$ (Pt. A in Fig. 10b). Penetrations of the background gas molecules are present further downstream; however, because of the low collision frequency, the presence of the background gas in this part of the free jet is not expected to cause significant change to the composition sampled at the extractor nozzle by the mass spectrometer.

The temperature of the argon in the free jet reaches the freezing point of $\approx 87^\circ\text{K}$ at $X/D \approx 7$ (pt. B in Fig. 10b). Thus, argon dimers may be formed. However, the collisions between argon atoms become so few that the chance of dimer formation is greatly reduced. The electron density curve in Fig. 10b is also calculated using isentropic relations with $\gamma = 5/3$. Based on the spectroscopically measured excitation temperature (8500°K) in the discharge chamber and subsequent correlation in the sonic reaction channel, the electron density at the channel exit is $\approx 1.7 \times 10^{15}$ e/cm³ and is calculated to be $\approx 4.8 \times 10^{12}$ e/cm³ at $X/D \approx 9$ (pt. C in Fig. 10b) where the electron density measured by the microwave interferometer is 4.2×10^{12} e/cm³ (pt. C' in Fig. 10b).

The interparticle collisions in the free jet are an important factor in correlating the data sampled at the extractor nozzle position downstream ($X/D = 14.4$) with the composition at the channel exit. The extent to which the plasma composition may be altered in the free jet depends on the accumulated number of collisions from the channel exit downward to the extractor nozzle. For Ar-Ar collisions (Fig. 10c), and most of the collision between argon and neutral reaction products, the accumulated number of collisions rises rapidly in the first nozzle diameter distance with little increase further downstream. The total number of the thermal collisions is estimated at ≈ 700 , sufficient to cause rotational and vibrational transitions, but not numerous enough to cause much excitation or ionization of the Ar atom or dissociation of reaction products. Also shown in Fig. 10c is the accumulated e - Ar collisions from the channel exit. The number of collisions are calculated from the established cross sections for low energy e - Ar interactions³⁰. The accumulated number of e - Ar collisions indicates an increasing trend reflecting a fairly constant collision frequency due to the Ramsauer-Townsend effect. For the conditions of this experiment it is reasonable to assume that the collision frequency between electrons and neutral reaction products is nearly the same as the e - Ar collision frequency. This means that electron attachment reactions may occur in the free jet. However, the electron density is reduced by two orders of magnitude because of isentropic expansion and consequently the attachment contribution in the free jet should be small compared with that in the reaction channel. In any case, to remove any doubt, electron attachment or electron ionization measurements should be performed using two channel lengths so it can be shown that the reactions are indeed occurring in the channel.

Microwave Interferometer Measurements of Electron Densities

An important parameter necessary to evaluate electron target molecule reactions is the electron density. Electron densities are measured with a Ka-band (27-40 GHz) microwave interferometer³¹ in the free jet region 2.5 cm from the exit plane as shown in Fig. 10. Open ended waveguides are used for antennas and are located so that the plasma is just outside of the antenna near field. An isolator is used behind the transmitting antenna to prevent reflections due to plasma scattering from entering the system. An additional isolator is placed behind the receiving antenna so the crystal detector behind the magic tee can be tuned to the incident received signal only and thus avoid reactive tuning due to the plasma path length. Precision phase shifters and attenuators are used throughout the circuit to obtain maximum accuracy and sensitivity.

The electron density and electron-neutral collision frequency are evaluated by relating the measured phase shift and attenuation due to the plasma to that predicted from a plane wave analysis assuming a parabolic electron density profile for a given diameter shown in Fig. 11. This system is capable of measuring electron densities from 2×10^{10} to 1×10^{13} e/cm³. Figure 12 shows the measured electron density as a function of rf generator power for various argon mass flow rates. Because the plasma is underdense, the electron-ion collision frequency is small compared to the interferometer signal frequency, no appreciable attenuation occurs. The measured electron densities in the free jet can be related to the electron densities in the channel as described in the preceding section. The electron density at the exit plane of the free jet at a mass flow of 0.22 g/sec and 57 kW of rf power was shown to be approximately 354 times higher than that measured 2.5 cm further downstream.

Mass Sampling System

The ion sampling system is shown schematically in Fig. 13. The center core flow of the expanded plasma plus target gas reaction products is sampled with a specially designed conical extractor nozzle. The cone angles of the extractor minimize boundary layer effects near the orifice and prevent gas particles from being scattered back into the expansion plume. The extractor is conduction cooled by water cooling its mounting flange. The extractor tip is located in the expansion region between the location of the transition zone and the Mach disc and contains a 250 μ m orifice through which the plasma is sampled. Mass analysis of the sampled plasma is achieved with a commercial quadrupole analyzer and ionizer (EAI 150A) located behind the extractor nozzle. Ion currents from the analyzer are collected with a Faraday cage and measured with an electrometer. Biasing on the input electrodes to the quadrupole and the Faraday cage is adjusted to optimize the positive or negative ion signal. Neutral species detection is accomplished by activating the internal filament and biasing supplies of the quadrupole control unit. Background pressures in the system during normal operation are 0.26 Torr in the expansion region and about 2×10^{-6} Torr in the analysis region. A sample of positive and negative ion data using SF₆ target molecules is shown in Fig. 14.

Interpretation of Experimental Measurements

Chemical rates for various kinds of reactions can often be evaluated by the use of a forward rate dominated model. For a forward dominated 2nd order process, the rate constant at temperature T is given by

$$K(T) = \frac{1}{t(n-N_0)} \ln \left[\frac{N_0[N(t) + n - N_0]}{n N(t)} \right]$$

where N_0 = initial reactant number density,
 $N(t)$ = reactant number density after reacting time t , and
 n = target molecule number density.

This forward rate dominated model assumes that the reactant number density depletion is due solely to the reaction of interest. If more than one new species are observed by the mass spectrometer, care must be exercised in using this model and in general the measured reaction rate will be an average for all the reactions observed.

Reactions involving the plasma free electrons are often of major interest in the study of plasma chemistry. In this case N_0 becomes the initial electron number density and $N(t)$ is the electron number density after reacting for time t ; $K(T)$ is

Figure 11 Electron Density (N) - Collision Frequency (V) Contour Plot

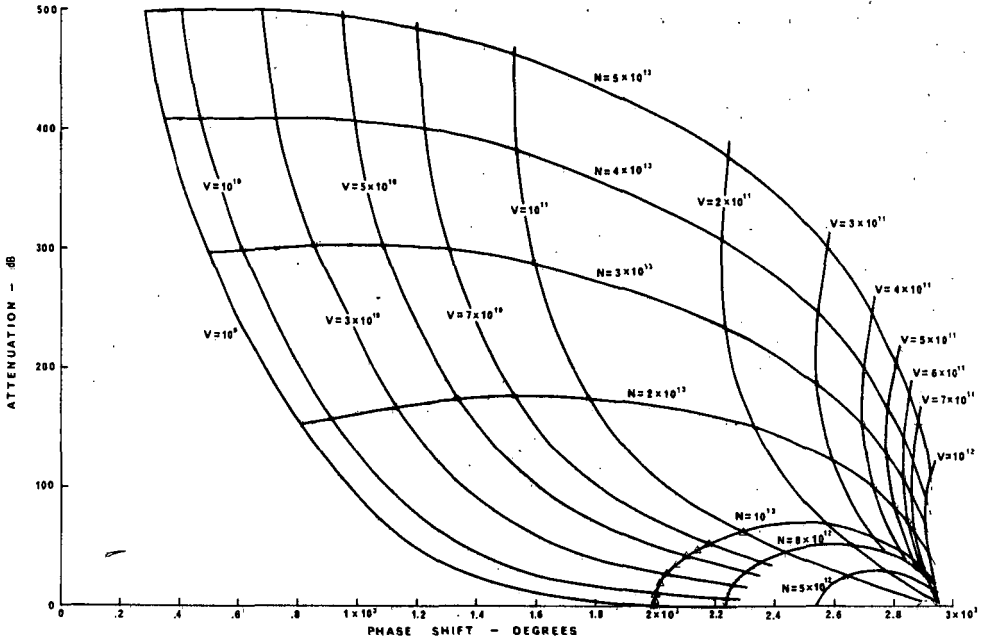


Figure 12 Measured Electron Densities

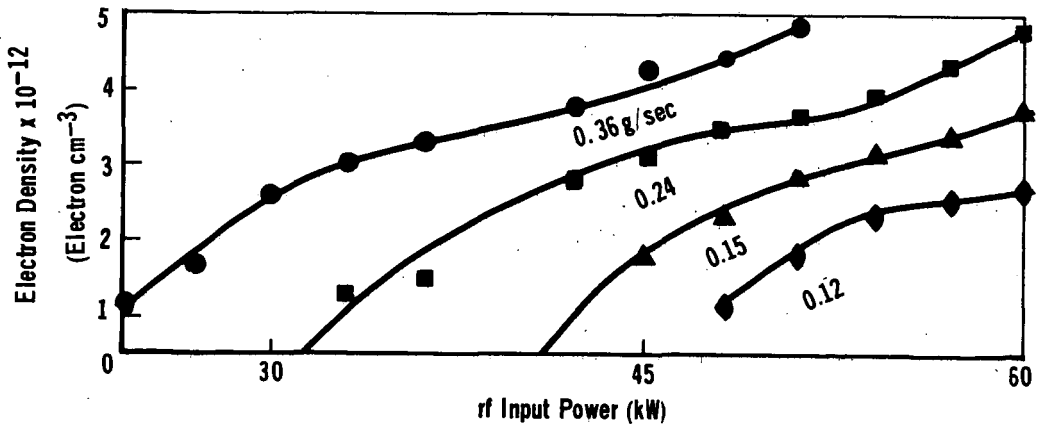


Figure 13 Schematic of Ion Sampling Systems

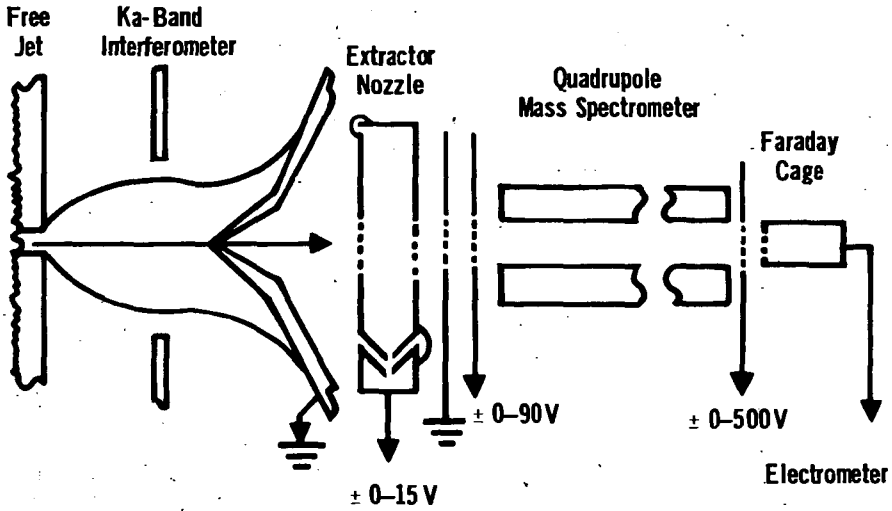
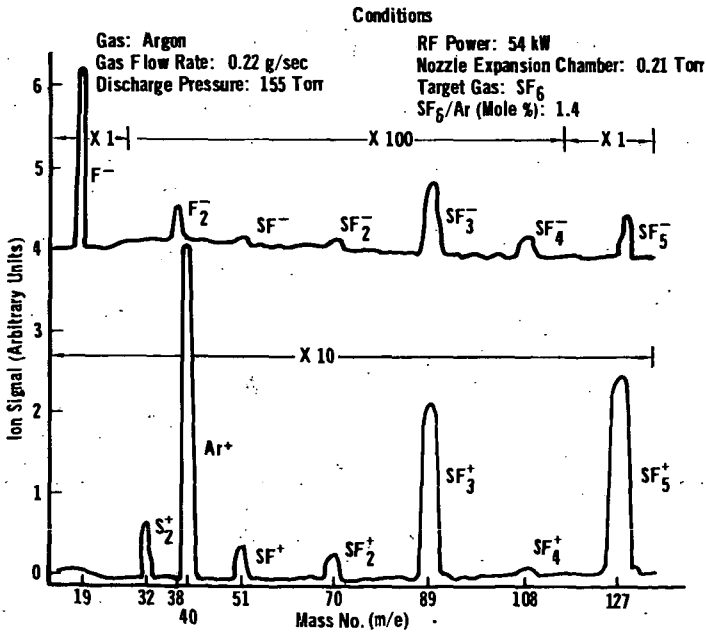


Figure 14 SF₆ Positive and Negative Ion Spectrum



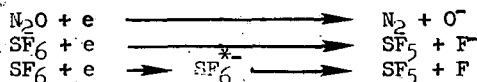
evaluated from the preceding equation. Therefore, this measurement technique provides a method for obtaining electron reaction rate constants at readily controllable temperatures. This rate constant can be compared to the theoretically predicted electron reaction cross sections $\sigma(T, E)^{32}$ by

$$K(T) = \frac{1}{m_e} \int_0^{\infty} \sigma(T, E) f(E) dE,$$

where $f(E)$ = electron energy distribution, and
 m_e = electron mass.

Since many investigators have found that the electron dissociative attachment cross section for some target molecules increases significantly with the target molecule temperature^{1,2}, the experimental apparatus described in this paper will extend these measurements to higher temperatures.

As an example, the dissociative attachment rate constant for



are evaluated at 3000°K. Electron temperatures for the experiment are assumed to be equal to the Ar excitation temperatures measured spectroscopically. Electron densities measured with the microwave interferometer and negative ion densities measured with the mass spectrometer are shown in Figs. 15 and 16. Note that for N₂O the rate of decrease of electron density approximately equals the rate of increase of negative ions. Since the plasma is less than 1% ionized the target molecule number density is usually much greater than the electron number density (i.e. $n \gg N_0$) and the equation for the second order rate reduces to

$$K(T) = \frac{1}{nt} \ln \frac{N_0}{N(t)}$$

From a plot of $\ln N_0/N(t)$ as a function of n, t $K(T)$ is evaluated.

The initial rate of increase of the F^- and SF_5^- is used to evaluate the rate constants when using SF_6 as a target gas. Initial slopes are usually used to evaluate the forward reaction rates because so few reaction products are formed at the low target gas mole fractions and consequently no appreciable reverse reactions appear. Measured reaction rates for various electrophilic target molecules are shown in Table III for a gas temperature of 3000°K.

Conclusions

A system has been developed for the measurement of chemical kinetics in high temperature plasmas. Plasma temperatures and electron densities have been measured in the reaction region. Reaction temperatures from 1000 to 3000°K have been attained. Direct measurements of reaction products including both positive and negative ion species and free electrons have been achieved. Electron attachment rate constants for several electrophilic target molecules have been calculated from the negative ion signals at a reaction temperature of 3000°K. Additional experimental attachment studies will be necessary to extend the measured attachment rates over a broad temperature range for comparison with data obtained by other investigators. Preliminary

Table III Measured Reaction Rates ($T_g = 3000K$)

| Probable Reaction | Estimated Rate $\times 10^{11}$ ($\text{cm}^3/\text{part. sec.}$) | Determined from |
|------------------------------------------------------------------------------------------|------------------------------------------------------------------------|--------------------------|
| $\text{Ar}^+ + \text{H}_2 \rightarrow \text{ArH}^+ + \text{H}$ | 6.3 | Ar^+ Decay |
| $\text{e} + \text{N}_2\text{O} \rightarrow \text{O}^- + \text{N}_2$ | 18 | O^- Increase |
| $\text{e} + \text{Br}_2 \rightarrow \text{Br}^- + \text{Br}$ | 13 | Br^- Increase |
| $\text{e} + \text{SF}_6 \rightarrow \text{F}^- + \text{SF}_5$ | 142 | F^- Increase |
| $\text{e} + \text{SF}_6 \rightarrow \text{SF}_6^{*-} \rightarrow \text{SF}_5 + \text{F}$ | 140 | SF_5^- Increase |

Figure 15 Electron Density and O^- Intensity

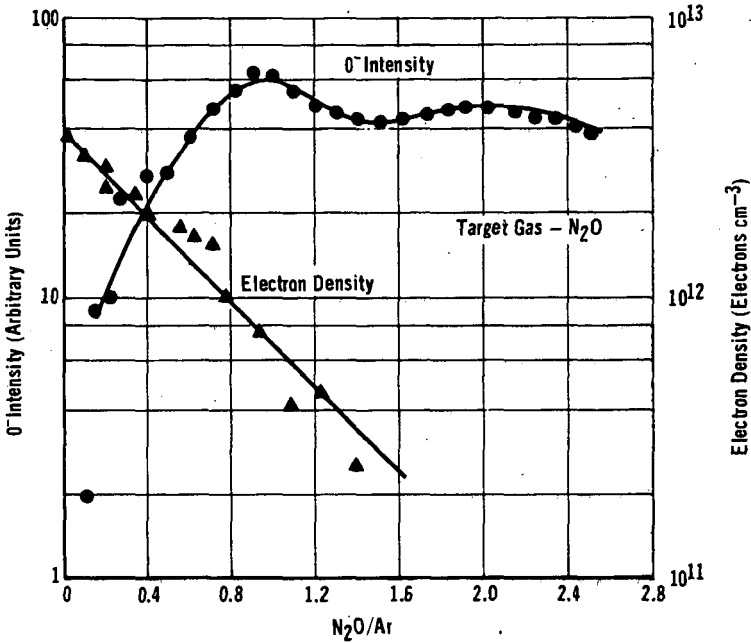
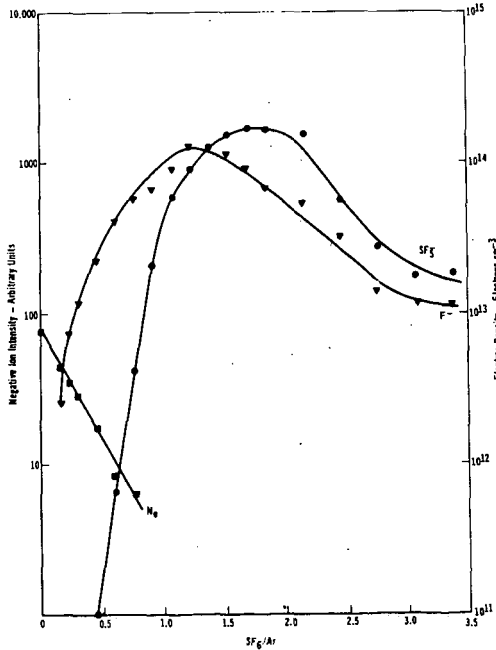


Figure 16 Negative Ion Intensity and Electron Density Using SF6 Target Molecules



results indicate that the electron attachment rates measured at 3000°K can differ significantly from those measured at lower temperatures.

Acknowledgment

The authors are indebted to Dr. R. A. Hefferlin for the optical spectrographic measurements of the source and reaction channel excitation temperatures and the electron density in the source.

References

1. P. J. Chantry, *J. Chem. Phys.* 51, 3369 (1969).
2. W. L. Fite and R. T. Brackman, Proceedings of the Sixth International Conference on the Ionization Phenomena in Gases (SERMA, Paris, 1963) Vol. 1, p. 21. W. L. Fite, R. T. Brackman and W. R. Henderson, Proceedings of the Fourth International Conference on the Physics of Electronic and Atomic Collisions (Science Bookcrafters, Inc., Hastings-on-Hudson, New York), p. 100.
3. W. R. Henderson, W. L. Fite and R. T. Brackman, *Phys. Rev.* 183, 157 (1969).
4. F. C. Fehsenfeld, A. L. Schmeltekopf, P. D. Goldan, H. I. Schiff and E. E. Ferguson, *J. Chem. Phys.* 44, 4087 (1966).
5. D. B. Dunkin, F. C. Fehsenfeld, A. L. Schmeltekopf and E. E. Ferguson, *J. Chem. Phys.* 49, 1365 (1968).
6. K. E. Starner, "Evaluation of Electron Quench Additives in a Subsonic Air Arc Channel," Aerospace Report TR-0200 (4240-10)-2 September 1968.
7. S. Atallah, W. A. Sanborn, A. Hoodbhoy, "The Effect of Chemical Additives on the Electron Density of Plasma Jets," AFCL 66-5, December 1965.
8. S. Aisenberg, "The Use of Chemical Additives for the Alleviation of the Plasma Sheath Problem," *Proceedings of the Conference on the Applications of Plasma Studies to Reentry Vehicle Communications, Vol. 1, (1967).*
9. J. H. Mullen, R. L. Cowperthwaite, and T. C. Peng, Twenty-Second Annual Gaseous Electronics Conference, Gatlinburg, Tennessee (1969), *Bull. Am. Phys. Soc.*, 51 3369 (1969).
10. T. B. Reed, *J. Appl. Phys.* 32, 821 (1961).
11. H. V. Eckert, F. L. Kelly and H. N. Olsen, *J. Appl. Phys.* 39, 1846 (1968).
12. R. Hefferlin, Progress in High Temperature Physics and Chemistry, (Pergamon Press, New York, 1969), Vol. 3, Chap. 2.
13. G. V. Marr, Plasma Spectroscopy (Elsevier, London, 1968).
14. W. Lochte-Holtgreven, Plasma Diagnostics, (North Holland Publishing Co., John Wiley & Sons, New York, 1968), Chap. 3.
15. G. Bekefi, Radiation Processes in Plasmas, (John Wiley, New York, 1966) Chap. 2.
16. R. H. Dicke, *Rev. Sci. Instr.* 17, 268 (1946).

17. D. B. Harris, *Microwave Journal*, 3 41, 47 (1960).
18. P. D. Strum, *PROC. IRE*, 48, 43 (1958).
19. J. S. Hey and V. A. Hughes, *PROC. IRE*, 48, 119 (1958).
20. G. G. Haroules and W. E. Brown III, *Rev. Sci. Instr.*, 38, 1043 (1967).
21. E. A. Ohm and W. W. Snell, *Bell System Tech. J.*, 42, 2047 (1963).
22. J. P. Appleton and K. N. C. Bray, *Fluid Mech.*, Part 4, 659 (1964).
23. S. C. Brown, Basic Data of Plasma Physics, (MIT Press, 1959), Chapter 1.
24. H. Schlichting, Boundary Layer Theory, (McGraw-Hill, 4th Ed. 1960), p. 35-36.
25. *Ibid*, p. 257.
26. G. N. Abramovich, Theory of Turbulent Jets, (MIT Press, Cambridge, Mass., 1963), p. 543.
27. *Ibid*, p. 544.
28. S. Crist, P. M. Sherman, D. R. Glass, *AIAA J.*, 4, 58 (1966).
29. J. B. French, *AIAA J.* 3, 993 (1965).
30. G. Francis, Ionization Phenomena in Gases, (Butterworth Scientific Publications, 1960), Chap. 2, p. 19.
31. M. A. Heald and C. B. Wharton, Plasma Diagnostics with Microwaves, (John Wiley, New York, 1965), Chap. 6 and 9.
32. T. F. O'Malley, *Phys. Rev.* 155, 59 (1967).